Journal of
Ship&Ocean
Technology
©MARCH 1999

SOTECH Vol.3; No.1, pp. 1~11

A Numerical Simulation for Contractive and Dilative Periodic Motion on Axisymmetric Body

Moon-Chan Kim

Daewoo Heavy Industries LTD., Seoul C.P.O. Box 6208, Korea

Abstract

Numerical simulation for the axisymmetric body with contractive and dilative periodic motion is carried out. The present analysis shows that a propulsive force can be obtained in highly viscous fluid by the contractive and dilative motion of axisymmetric body. An axisymmetric code is developed with unstructured grid system for the simulation of complicated motion and geometry. It is validated by comparing with the results of Stokes approximation with the problem of uniform flow past a sphere in low Reynolds number($R_n = 1$). The validated code is applied to the simulation of contractive and dilative periodic motion of body whose results are quantitatively compared with the two dimensional case. The simulation is extended to the analysis of waving surface with projecting part for finding out the difference of hydrodynamics performance according to variation of waving surface configuration. The present study will be the basic research for the development of the propulsor of an axisymmetric *micro-hydro-machine*.

Keywords : axisymmetric analysis, contractive and dilative motion, highly viscous fluid, unstructured method

1 Introduction

Most of animals living in water or in air move by the mode of locomotion. It finds best suited to its particular environment and ecology [Alexander, 1992]. Even the same fluid environment is felt stickier by a small animal than by a large one: below a certain size the effect of fluid viscosity becomes larger than the effect of its inertia. To micro-organisms, water is a highly resistive fluid, and swimming in it must be felt as swimming in honey. Under this condition, it is difficult to obtain a thrust by a local propulsion such as fanning or jetting which may be equivalent to propeller or water jet for ship. Although various kinds of propulsive motion are observed in the micro-organisms [Alexander, 1992 & Azuma, 1992], the common feature is that they gain thrust by moving their whole body in order to generate thrust which is over the frictional resistance of high viscosity of surrounding fluid.

Contractive and dilative periodic motion is one of the whole body motions in micro-organisms. Some micro-organisms use this motion for obtaining a propulsive force [Baba, 1974]. Trochoidal motion can be applied to the waving surface of contractive and dilative motion. The trochoidal motion can be actually seen in the movement of ciliary [Kinoshita, 1967] as shown in Fig.1 where ciliary motion can be formed by the movement of ciliary end: the.advancing direction is the same

as the propagating direction. A propulsive force is derived by power strokes while recovery stokes bring a drag. As the recovery strokes are shorter than the power strokes, a propulsive force can be obtained by the trochoidal motion.

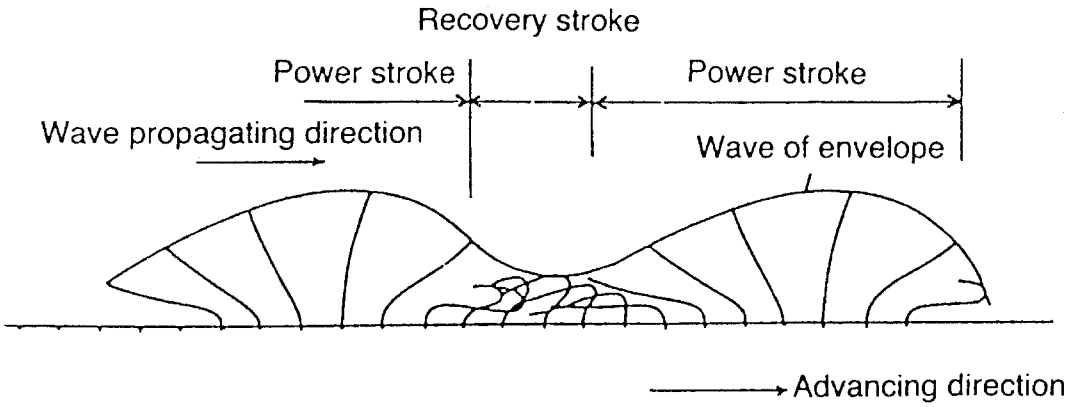

Figure 1. Trochoidal motion by the end of ciliary

On the other hand, with the progress of computational fluid dynamics, the study of complicated motion can be numerically carried out by the enhancements in computer capability as well as grid generation technique. The progress of CFD with unstructured grid has been successfully carried out at various fields of engineering [Roe, 1981 & Barth et al., 1989]. According as the unstructured grid becomes popular, complicated configuration of body and/or motion are no more difficult to solve by the numerical computations.

The purpose of the present research is to study the mechanism of thrust by contractive and dilative motion of axisymmetric body for the development of *micro-hydro-machine* which is a small robot working in highly viscous fluid. In the previous studies [Kim et al., 1998 & Kim et al., 1997], the two dimensional analysis of contractive and dilative motion of body has been carried out for finding out the possibility of obtaining a propulsive force in highly viscous fluid. In the present study, the analysis is extended to the axisymmetric body to prove that the contractive and dilative motion is still an effective propulsive motion for obtaining a propulsive force in three dimensional field. In the present axisymmetric analysis, the effectiveness of the contractive and dilative motion is shown in highly viscous fluid although it is a little less than that of the two dimensional case. With refering a lobster's propulsive mechanism, the projections case of contractive and dilative motion of axisymmetric body is also treated to compare with the smooth surface. The present simulation is expected to be extended to the study for finding the optimized configuration of waving surface. The developed axisymmetric analysis code is first validated by the problem of uniform flow past a sphere, for which the Stokes approximated solution can be available for the comparison. The validated code is applied to the simulation of contractive and dilative motion of axisymmetric body with smooth surface as well as with projecting parts. The present study will be useful for the development of the propulsor of an axisymmetric *micro-hydro-machine*.

2 Formulation and Validation

2.1 Formulation and transport theorem

Navier-Stokes equation for the axisymmetric case can be formulated in vector expression of conservative form [Hoffmann et al., 1993] as

$$\frac{\partial \mathbf{p^a}}{\partial t} + \frac{\partial \mathbf{q^a}}{\partial \tau} + \mathbf{P}(\frac{\partial \mathbf{f^a}}{\partial x} + \frac{\partial \mathbf{g^a}}{\partial r} + \mathbf{h}) + \mathbf{Q}(\frac{\partial \mathbf{f_v^a}}{\partial x} + \frac{\partial \mathbf{g_v^a}}{\partial r} + \mathbf{h_v}) = 0 \tag{1}$$

where,

$$\mathbf{p^a} = \begin{bmatrix} 0 \\ u \\ v_r \end{bmatrix} \mathbf{q^a} = \begin{bmatrix} p \\ u \\ v_r \end{bmatrix} \mathbf{f^a} = \begin{bmatrix} u \\ u^2 + p \\ uv_r \end{bmatrix} \mathbf{g^a} = \begin{bmatrix} v_r \\ uv_r \\ v_r^2 + p \end{bmatrix}$$

$$\mathbf{f_v^a} = \begin{bmatrix} 0 \\ \frac{4}{3}\frac{\partial u}{\partial x} - \frac{2}{3}\frac{\partial v_r}{\partial r} \\ \frac{\partial u}{\partial r} + \frac{\partial v_r}{\partial x} \end{bmatrix} \mathbf{g_v^a} = \begin{bmatrix} 0 \\ \frac{\partial u}{\partial r} + \frac{\partial v_r}{\partial x} \\ \frac{4}{3}\frac{\partial v_r}{\partial r} - \frac{2}{3}\frac{\partial u}{\partial x} \end{bmatrix}$$

$$\mathbf{h} = \frac{1}{r}\begin{bmatrix} v_r \\ uv_r \\ v_r^2 \end{bmatrix} \mathbf{h_v} = \frac{1}{R_n r}\begin{bmatrix} 0 \\ \frac{\partial u}{\partial r} + \frac{1}{3}\frac{\partial v_r}{\partial x} \\ \frac{4}{3}\frac{\partial v_r}{\partial r} - \frac{2v_r}{r} \end{bmatrix} \mathbf{P} = \begin{bmatrix} \beta^2 & 0 & 0 \\ 0 & 1 & 0 \\ 0 & 0 & 1 \end{bmatrix} \mathbf{Q} = \begin{bmatrix} 0 & 0 & 0 \\ 0 & \frac{1}{R_n} & 0 \\ 0 & 0 & \frac{1}{R_n} \end{bmatrix}$$

where r is radial coordinate and v_r is radial velocity component. For the analysis of moving problem, the effect due to the movement of control volume should be considered. Spatial integration of the Navier-Stokes equation over the control volume around cell i gives the following equations,

$$\iint_{V_i} (\frac{\partial \mathbf{p^a}}{\partial t} + \frac{\partial \mathbf{q^a}}{\partial \tau} + \mathbf{R}) dV = 0 \tag{2}$$

where V_i is the control volume and

$$\mathbf{R} = \mathbf{P}(\frac{\partial \mathbf{f^a}}{\partial x} + \frac{\partial \mathbf{g^a}}{\partial r} + \mathbf{h}) + \mathbf{Q}(\frac{\partial \mathbf{f_v^a}}{\partial x} + \frac{\partial \mathbf{g_v^a}}{\partial r} + \mathbf{h_v}) \tag{3}$$

By the transport theorem [Newman, 1977], the time derivative of the volume integral is given by

$$\frac{\partial}{\partial t}\iint_{V_i} \mathbf{h} dV = \iint_{V_i} \frac{\partial \mathbf{h}}{\partial t} dV + \oint_{\partial V_i} \mathbf{h}(u_g n_x + v_g n_y) dS \tag{4}$$

where ∂V_i is edges surrounding the control volume of cell i, $(n_x,\ n_y)$ and $(u_g,\ v_g)$ are $(x,\ y)$ components of the outward unit normal vector of ∂V_i and the grid velocity, respectively. The effect of the movement of control volume is considered by equation (4).

2.2 Validation

The developed axisymmetric code is validated by the problem of uniform flow past a sphere, for which the Stokes solution is available for the comparison because its solution is the exact one if R_n is equal or below 1.0. This problem is adequate for the validation of axisymmetric developed code even though it is steady. The essential feature of the Stokes approximation is that all the convective inertia components are assumed to be small compared to the viscous forces. The Stokes approximation is precisely described in the reference [Currie, 1974]. The nondimensional velocity and pressure distribution are given by

$$u = [n_x - \frac{1}{4}\frac{a}{r}(\frac{a^2}{r^2} + 3)n_x + \frac{3}{4}\frac{ax}{r^2}(\frac{a^2}{r^2} - 1)n_r] \tag{5}$$

$$p = -\frac{3}{2}R_n\frac{ax}{r^3} \tag{6}$$

It is radially confirmed that equation(5) satisfies the boundary condition $u = 0$ over the entire surface $r = a$. The magnitude of the force acting on the sphere is

$$C_D = \frac{24}{R_n} \tag{7}$$

where $R_n = \rho U 2a/\mu$ is the Reynolds number.

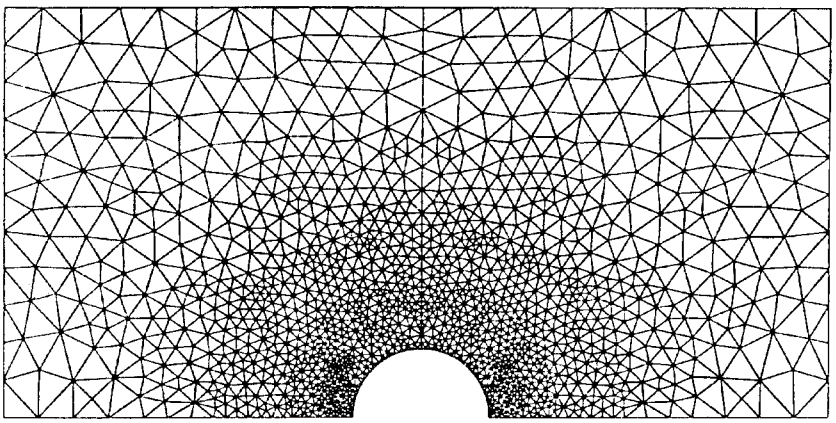

Figure 2. Generated grid for the problem of uniform flow past a sphere(no. of grid = 2658, grid-A)

The generated grid for the validation is shown in Fig.2. No-slip condition is imposed on the surface of sphere. The length and the velocity is nondimensionalized by the diameter of sphere and on-coming velocity U respectively. The comparison of u-velocities between the Stokes solution and the computation along $x = 0$ plane is shown in Fig.3 where an excellent agreement is seen between the two. The forces are shown in Table 1. As the grid becomes finer, the results of force is almost the same as the Stokes soultion. Even in the coarse grid(almost one third of the finer grid), the computed results are not much different from that of Stokes approximation and as the grid becomes coarser, the both values of friction and pressure becomes lower than those of the finer grid case.

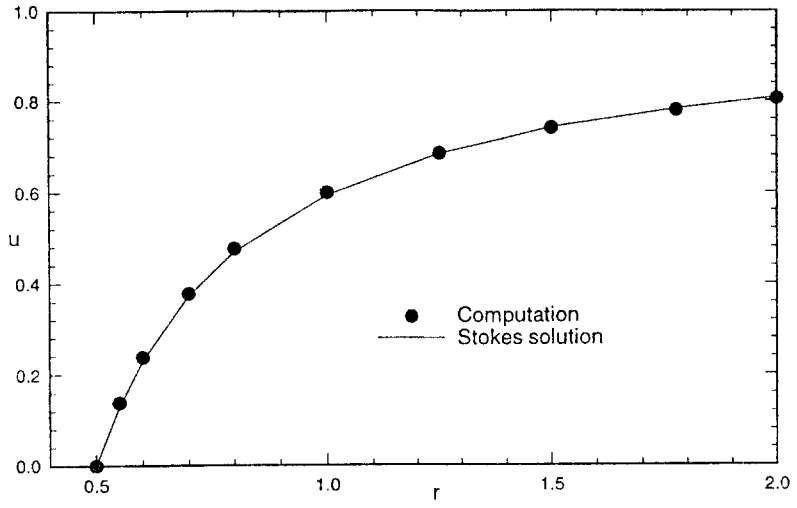

Figure 3. Comparison of u-velocity between the present computation(no. of grid=2658) and Stokes solution at $x = 0$.

Table 1. Comparison of forces acting on the sphere at $R_n = 1$.

		frictional force	pressure force	total force(C_D)
Stokes solution		16.00	8.00	24.00
computations (no. of grid)	2658	14.88	7.80	22.68
	7528	15.86	8.12	23.98

In the following computations, the nondimensional force coefficients for an axisymmetric body is defined by

$$C_f^{3d} = \int_0^1 \int_0^{2\pi} C_f r(x) d\theta dx \tag{8}$$

$$C_p^{3d} = \int_0^1 \int_0^{2\pi} C_p r(x) d\theta dx \tag{9}$$

where $r(x)$ is the radius at x.

3 Computations

3.1 Description of motion

An axisymmetric model is adopted for the application of contractive and dilative motion as shown in Fig.4. The middle part of the body makes contractive and dilative perodic motion which might be so called as a worm-like motion, while the head and tail parts are not movable. The Reynolds number is defined by the length(L) of the movable part and the phase velocity($V_p = \frac{\omega}{k}$) of motion. All the lengths are non-dimensionalized by the length(L) of movable part of body. Trochoidal

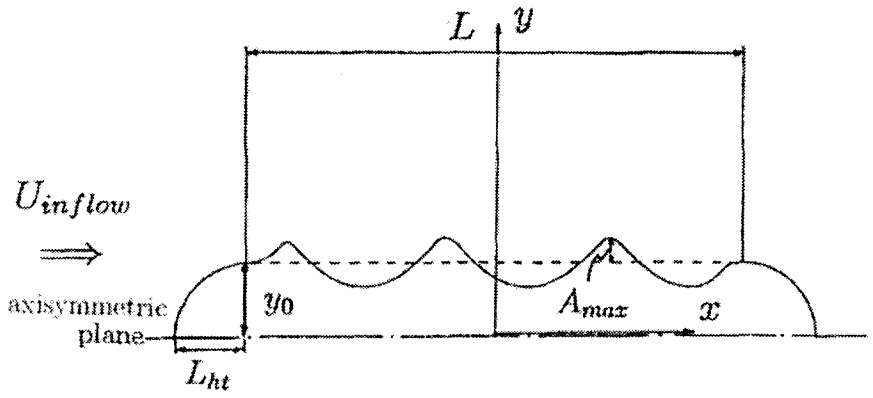

Figure 4. Schematic for the description of the contractive and dilative motion of axisymmetric body.

motion is applied to the waving surface of the body. The surface position(x', y') of trochoidal motion is defined by equations(10) and (11).

$$x' = x + A(x)b\cos(kx + \omega t)/L \tag{10}$$

$$y' = y_o + A(x)\sin(kx + \omega t)/L \tag{11}$$

In the present study, it is set as $k = 6\pi$, $w = 6\pi$, $b = 0.5$ and $y_o(= L_{ht}) = 0.15$. As shown in equations(10) $\sim$ (11), the trochoidal direction is the same as the advancing direction. A window function is used to match the moving part with the fixed part in amplitude $A(x)$. Matching zone(L_D) is set to be 10% of the length(L) of waving surface and the third order polynomial is used for window functions in the matching zone as follows:

$$\begin{aligned} A(x) &= \frac{3A_{max.}}{L_D^2}x^2 - \frac{2A_{max.}}{L_D^3}x^3, && 0 \le x < L_D \\ A(x) &= A_{max.}, && L_D \le x < L - L_D \\ A(x) &= \frac{3A_{max.}}{L_D^2}(L-x)^2 - \frac{2A_{max.}}{L_D^3}(L-x)^3, && L - L_D \le x \le L \end{aligned} \tag{12}$$

The generated grid points above waving surface is proportionally shrunk or stretched due to the movement of the waving surface as following equations.

$$x_i^{n+1} = x_i^n + A(x_i^n)b(\cos(kx_i^n + \omega t) - \cos(kx_i^n + \omega(t + \Delta t))) \tag{13}$$

$$y_i^{n+1} = y_u + \frac{d^{n+1}(x_i) - y_u}{d^n(x_i) - y_u}(y_i^n - y_u) \tag{14}$$

where $d(x_i)$ is the length between the base of body surface(y_u) and the top location(h) at $x = x_i$ and n is the previous time step.

3.2 Smooth surface

The generated grids for the axisymmetric computations with smooth surface are shown in Fig.5. The phase velocity of the waving surface is ten times the on-coming velocity and amplitude of

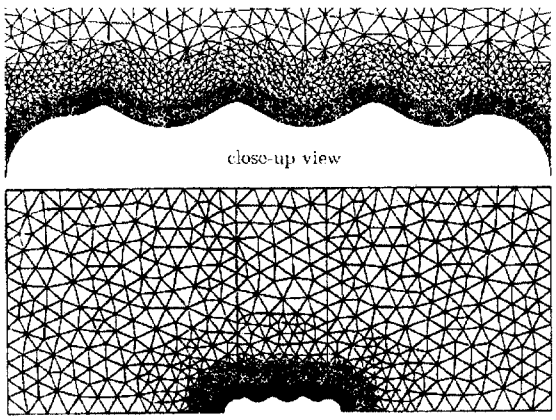

Figure 5. Generated grid of smooth surface case for the analysis of axisymmetric contractive and dilative motion.

Table 2. Summarized results of computed x-directional mean forces.

dimension	kind of surface	R_n	C_f^{3d}	C_p^{3d}	C_t^{3d}
two dimension	smooth surface	50	-0.370(C_f)	0.349(C_p)	-0.021(C_t)
axisymmetry	smooth surface	5	-2.633	1.216	-1.417
		50	-0.325	0.542	0.217
	right projection	5	-2.071	0.636	-1.435
		50	-0.218	0.119	-0.099
	left projection	5	-2.407	0.821	-1.586
		50	-0.242	0.145	-0.097

waving motion is set to be 3% of the body length(L). Computations are carried out at two different Reynolds numbers of 5 and 50. The number of physical time step(Δt) per a cycle is set to be 60 and the number of iteration for pseudo time is 6000. The computed mean forces are summarized in Table 2 which are obtained by the time average in last one cycle. Two dimensional computation is also carried out to compare quantitatively with the axisymmetric case. Computing conditions for the two dimensional case are set to be the same as the axisymmetric conditions. The portion of pressure force in axisymmetric case becomes larger than that of the two dimensional case as seen in Table 2. For the axisymmetric case at $R_n = 50$, the total force is acting as a drag while the total force of two dimensional case is acting as a propulsive force. As the Reynolds number becomes lower, the frictional force coefficient becomes much larger compared with the increase of pressure coefficient as shown in Table 2. This tendency is the same in two dimensional case. As the portion of pressure drag is comparatively larger than two dimensional case, more optimized motion and/or surface configuration is expected to be studied. In the present study, as mentioned before, the case of surface with projecting part is also tried to be computed to find out the possibility of finding out the optimized configuration.

The computed velocity vectors and pressure contours at $R_n = 50$ are shown in Fig.6 $\sim$ Fig.7. The figures are displayed at after 5 cycles of computation. The rotating effect is also seen in

the Fig.6, by which a frictional force can be used for obtaining a propulsive force. The pressure between on the uphill and on the downhill of waving surface is acting as a drag to the body because the propagating direction of trochoidal motion is contrary to the direction of the oncoming flow, whose tendency is the same as the two dimensional case[Kim et al., 1998].

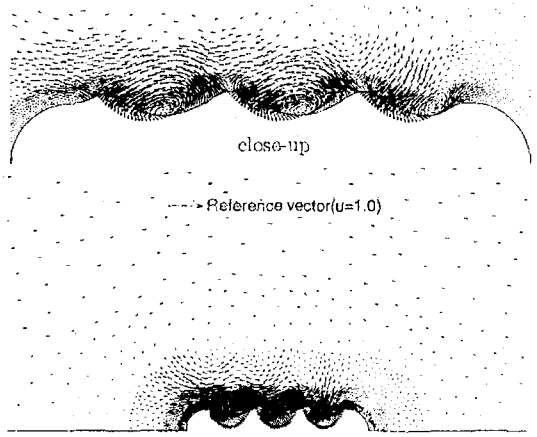

Figure 6. Computed velocity vectors for the smooth surface case at $R_n = 50$.

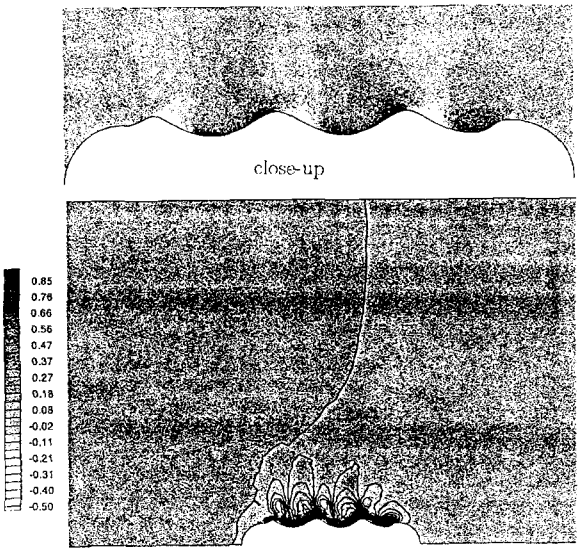

Figure 7. Computed pressure contours for the smooth surface case at $R_n = 50$.

3.3 Surface with projecting part

The simulation of contractive and dilative motion with attached projecting part is carried out to study the hydrodynamics performance according to the variation of surface configuration. In the present study, the simple configurations of projecting part is treated whose profiles are quarter circle as shown in Fig. 8.

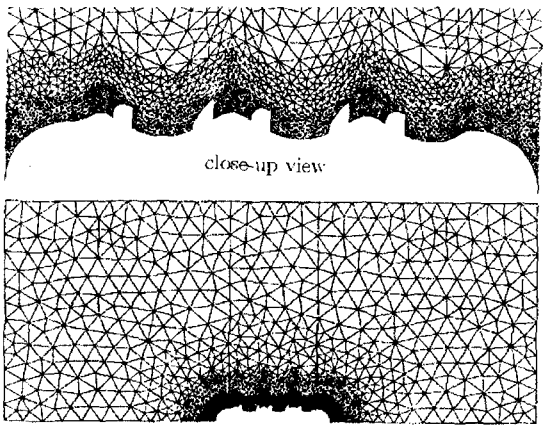

Figure 8. Generated grid of right projection case for the analysis of axisymmetric contractive and dilative motion.

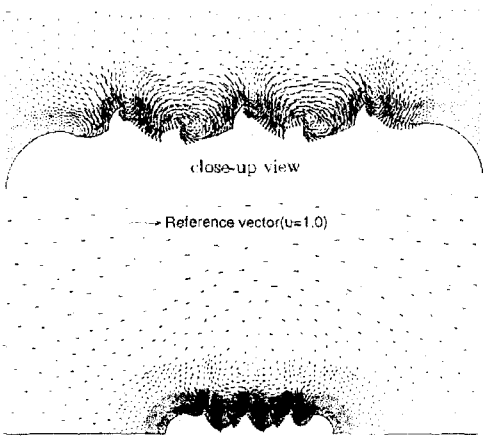

Figure 9. Computed velocity vectors for the right projection case at $R_n = 50$.

The trochoidal motion is imposed on the waving surface where the projecting part of quarter circles are deformed according to the waving surface. Left projection whose shape is longitudinally reverse to the right projection, is also computed. The parameters of computations are set to be the same as those of smooth surface for comparison.

The computed forces are tabulated in Table 2. The frictional propulsive force and the pressure drag of right and left projections are smaller than those of smooth surface. This tendency is more clear in the right projection. In other words, although the frictional propulsive force of the projection's case is smaller than that of smooth surface, the total propulsive force is a little larger than that of the smooth surface at $R_n = 50$ because the pressure drag of the projection's case is much smaller. At the Reynolds number of 50, the difference of total force between the right and the left projection is not clearly seen. As the Reynolds number becomes smaller($R_n = 5$), the advantage of using projecting part is not clearly seen. It can be said that the projecting part more effectively works in the range of $R_n \geq 50$.

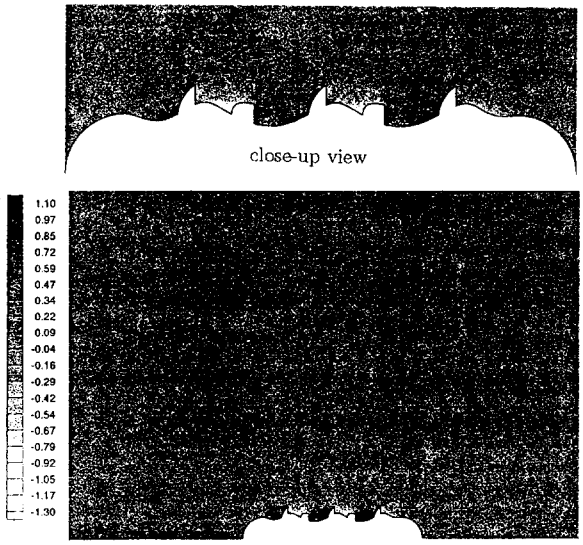

Figure 10. Computed pressure contours for the right projection case at $R_n = 50$.

The computed velocity vectors and pressure contours of right projection case are shown in Fig.9 $\sim$ Fig.10. The velocity vectors of projection's case is more complicated than that of smooth surface case as expected. The rotating effect by the trochoidal motion seems less than that of smooth surface case because of the projecting part. In the pressure contours, the difference between the surface with projecting part and with smooth surface is clearly seen. As the pressure on the right side of projecting part when it goes in low position, is locally high because of the trochoidal mechanism, it pushes the body in forward direction. Therefore the total pressure drag acting on a body becomes less than that of smooth surface by this paddle-like mechanism. The most optimized configuration for the present motion is expected to be studied in a future work.

4 Conclusions

Axisymmetric analysis for the contractive and dilative periodic motion of body is carried out. The present analysis shows the possibility of obtaining a propulsive force in three dimensional highly viscous fluid by the contractive and dilative motion of axisymmetric body. The unstructured code is developed for the simulation of contractive and dilative motion of axisymmetric body.

Contractive and dilative motion of axisymmetric body with smooth surface is first simulated by the developed code. In the three dimensional field, the frictional force can be also used for obtaining a propulsive force by trochoidal motion although the portion of pressure drag is a little larger than that of the two dimension. The simulation is extended to the analysis of surface with projecting part to study the hydrodynamics performance according to the variation of surface configuration. According to the mechanism of the projecting part, the frictional propulsive force as well as pressure drag becomes smaller than those of smooth surface. At the $R_n = 50$, the gain by the projecting part is shown in the present computation. According as the Reynolds number becomes smaller($R_n \leq 50$), the smooth surface is better for obtaining a propulsive force.

The present study will be the basic research for the development of the propulsor of an ax-

isymmetric *micro-hydro-machine.*

References

1. Alexander, R. M., 1992, Exploring Biomechanics(animal in motion), W.H. FREEMAN AND COMPANY.
2. Azuma, A., 1992, The Biokinetics of Flying and Swimming, Springer-Verlag.
3. Baba, S. A., 1974, Development changes in the pattern of ciliary response and swimming behavior in some invertebrate larvae, Swimming and flying in nature, Vol.1 Plenum, New York.
4. Kinoshita, H. and Murakami, A., 1967, Control of ciliary motion, Physiol Rev. Vol.47.
5. Roe, P. L., 1981 Approximate Riemann Solver, Parameter vectors and Difference scheme, Journal of Computational Physics, Vol.43.
6. Barth, T. J., Jespersen, D. C., 1989, The Design and Application of Upwind Scheme on Unstructured Meshes, AIAA paper 89-0366.
7. Kim, M.-C., Ninomiya, S., Mori, K., Doi, Y., 1998, A Study on a Propulsion System by Peristaltic Motion in Highly Viscous Fluid, Proceedings of 22nd Symposium of Hydrodynamics, Washington D.C..
8. Kim, M.-C., Mori, K., Xu, Q., Doi, Y., 1997, A Numerical Scheme with Unstructured Moving Grid System and Its Application to Two-Dimensional Complicated Flow, Journal of The Society of Naval Architecture of Japan, Vol.181.
9. Hoffmann, K. A., Chiang, S. T., 1993, Computational Fluid Dynamics for Engineers, ISBN 0-9623731-8-4, Engineering Education System.
10. Newman, J. N., 1977, Marine Hydrodynamics, The MIT Press.
11. Currie, I. G., 1974, Fundamental Mechanics of Fluids, McGRAW-HILL.